Thermally-induced all-damage-healable superhydrophobic surface with photocatalytic performance from hierarchical BiOCl

Shanshan Jia[a], Yao Lu[b], Sha Luo[a], Yan Qing[a,c,*], Yiqiang Wu[a,c,*], Ivan P. Parkin[d]

[a] College of Materials Science and Engineering, Central South University of Forestry and Technology, Changsha 410004, China

[b] Department of Mechanical Engineering, University College London, London, WC1E 7JE, UK

[c] Hunan Provincial Collaborative Innovation Center for High-efficiency Utilization of Wood and Bamboo Resources, Central South University of Forestry and Technology, Changsha 410004, P. R. China

[d] Department of Chemistry, University College London, 20 Gordon Street, London, WC1H 0AJ, UK

[*] Corresponding author

Email address: qingyan0429@163.com or wuyq0506@126.com

Abstract: Preparation of superhydrophobic surfaces capable of recovering both the surface chemistry and hierarchical structure is still a challenge. In this work, all-damage-healable superhydrophobic surface was fabricated by assembly of superhydrophobic and hierarchical BiOCl on lignocellulosic substrates. Fibers having thermally responsive behavior, the main component of lignocellulosic materials, act as the underlying movable substrates. By a simple heating treatment, fibers can convey the undamaged neighbored superhydrophobic coating to the damaged area. In

this way, the loss of superhydrophobicity caused by rigorous mechanical destructions, even deep cuts of one hundred of micrometers wide, can be restored, mimicking the self-healing mechanism of human skin. Superior self-healing ability in surface chemistry was also confirmed. Meanwhile, the as-prepared superhydrophobic surfaces demonstrated reliable photocatalytic ability, a useful property for resisting organic contaminations. Interestingly, it was found that the photocatalytic activity can be enhanced by tuning the surface wettability. This work reported the first use of substrate material's inherently thermally responsive property to demonstrate self-healing superhydrophobic surface with photoctalyticity, which not only promotes the application of superhydrophobic materials in complex environment, but also opens up a new perspective in designing durable superhydrophobic materials.

Keywords: superhydrophobic surface, biomimetic, all-damage-healable, lignicellulose, controllable photocatalytic property

1. Introduction

Lignocellulose is a kind of abundant, renewable, environmentally friendly biopolymer. It is an important raw material for industrial and daily life applications (e.g., furniture).[1-5] Integrating new functions into the lignocellulose-based materials is an attractive research direction. For example, superhydrophobic lignocellulosic materials could find exciting applications in decoration, medical devices, functional clothing, and green electronic devices.[6-14] However, preparing lignocellulosic materials with a stable superhydrophobic surface is still extremely challenging. Previous efforts usually render superhydrophobic surfaces that cannot last long under

contamination or mechanical pressure.[15-18] A promising strategy to circumvent the above problems is to engineer superhydrophobic surfaces that can self-heal after being damaged.[19-20] The famous concept to construct self-healing superhydrophobic surfaces onto lignocellulostic materials is embedding healing agents (i.e., low surface energy materials) into the porous substrates. Once the outmost hydrophobic layer is damaged, the underneath healing agent can migrate to the damaged area and restore it. The migration process is usually activated by an external stimulus, such as heating treatment, light irradiation and water exposure.[21-25] Nevertheless, these approaches used in previous studies are only effective in recovering surface chemistry. When surface microstructure is destroyed by severe mechanical destructions, such as wide and deep scratches, and abrasions, these healing approaches usually fail.[26] A superhydrophobic surface that can repair both hydrophobic layer and hierarchical structure would be more favorable for complex practical applications.

Inspired by the powerful self-healing mechanism of a wound on human skin,[27-28] Wu et al.[29] fabricated a self-healing superhydrophobic film through depositing superhydrophobic conductive composite layer on a thermally responsive polycaprolactone (PCL)/poly(vinyl alcohol) (PVA) composite film. Once its superhydrophobicity was damaged by wide and deep scratches, the undamaged superhydrophobic coating could be conveyed to the damaged area via the migration of the underlying film after activated by electrothermal heating or near-infrared light irradiation. Actually, fibers, the main component of lignocellulosic materials, have thermal responsive property. Therefore, if superhydrophobic coating can be rationally

assembled on fibers, superhydrophobic surface with self-healing ability in both surface structure and chemistry can be anticipated.

Organic contamination induced superhydrophobic property degradation is also a huge problem in practical applications.[30-31] Photocatalysts such as TiO_2, ZnO_2 and CuInZnS are effective for the removal of oily dirt and even toxic gas via photocatalytic self-cleaning effect.[32-36] Inserting photocatalysts into superhydrophobic surfaces should be a promising method to solve the superhydrophobic stability issue towards organic contamination.[30, 37] BiOCl is a promising photocatalyst with advantages, such as high reactivity, nontoxicity, high stability, and preparation at a low-cost.[38-39] Nevertheless, as far as we know, embedding BiOCl nanomaterials into the superhydrophobic surface for design of self-healing and photocatalytic properties has not yet been reported.

Herein, we demonstrated an all-damage-healable superhydrophobic surface with photocatalyticity by assembly of superhydrophobic and hierarchical BiOCl on wood. By a simple and short heating treatment, the thermally responsive fiber could convey the top superhydrophobic coating to the damaged area via its own movement. In this way, the restoration of the loss of superhydrophobicity caused by mechanical damages, even wide and deep cuts, was achieved. To the best of our knowledge, this is the first report on recovering the damaged microstructure via utilizing substrate material's inherently thermally responsive property. Excellent self-healing ability in surface chemistry was also proved. The as-prepared superhydrophobic surface also possessed photocatalytic ability. More interestingly, it was found that the photocatalytic activity

could be enhanced by tuning surface water repellency.

2 Materials and methods

2.1 Materials

Bismuth chloride ($BiCl_3$), poly (vinylpyrrolidone) (PVP), and citric acid monohydrate (38%) were purchased from Nation Reagent Co., Ltd (China). Hydrochloric acid (HCl) was provided by Shenzhen City Hengli Chemical Co., Ltd. Perfluorooctyltriethoxysilane (PFOTS) was obtained from Tokyo Chemical Industry Co., Ltd. Rodamine B (RhB) dye was provided by Tianjin kwangfu Fine Chemical Industry Research Institute (China). Ethanol (EtOH) was got from Tian Jin Damao Chemical Reagent Co, Ltd. All reagents were used as received without further purification.

2.2 Method

Preparation of BiOCl nanocrystals: The method used for preparing BiOCl nanocrystals was following previous reports.[40] Briefly, 11.8 g $BiCl_3$ was first added into 200 g distilled water. Then, 24.6 ml of HCl was added into the above solution. Under vigorous stirring at room temperature for 30 min, a homogeneous solution was obtained. In order to tune the concentration of $BiCl_3$ to 0.15 M, the above homogenous solution was transferred into 250 ml-volumetric flask and then increased the volume of $BiCl_3$ solution to 250 ml by adding a certain amount of distilled water. The target sample $BiCl_3$ solution was prepared.

Next, 42 g distilled water, 0.001g PVP, and 11 g citric acid were dissolved into 50 ml ethanol. After heated at 80 ^oC for 5 min, 10 ml of 0.15 M $BiCl_3$ solution was

added slowly into the mixture under stirring. Then, the obtained solution was transferred into in a sealed container and stirred for another 3 h at 80 ^{o}C.

Finally, the production of the second step was purified by rinsed with water and ethanol for 6 times. BiOCl nanocrystals were obtained after drying the purified production at 80^{o}C in vacuum for 8h.

Fabrication of self-healing superhydrophobic surface: The self-healing superhydrophobic surface was fabricated by assembly of superhydrophobic and hierarchical BiOCl on lignocellulosic material. Specifically, 0.5g PFOTS was dissolved in 20 g ethanol by magnetic stirring for 1.5 h. A certain amount of BiOCl was dispersed in 5 g ethanol by strong sonication (200 W) for 10 min using an ultrasonic cell disruptor. The molar ratio between PFOTS and BiOCl was 10:1. Then, the BiOCl solution was added into the above PFOTS solution by ultrasonic agitation for 0.5 h to obtain a homogeneous reactant solution. Wood, as a typical and representative lignocellulosic material, was used as substrate. The wood substrate together with the reactant solution (1.5 mL/cm^2) was placed into a weighing bottle with a diameter of 25 mm. It should be noted that the substrate was completely encircled by liquid to guarantee enough ethanol preserved in wood. Next, the small bottle was transferred into a 250-mL jar under a semi-sealed state and heated at 100^{o}C. Superhydrophobic samples were fabricated after 1.5 h. The obtained samples were named as “Bi&F-wood”. The detailed synthesis process was illustrated in Figure 1a. Wood samples treated with the solution only containing BiOCl nanocrystals were also prepared, which were named as “Bi-wood”. The preparation process of Bi-wood was

the same as that of Bi&F-wood.

2.3 Characterization

The scanning electron microscopy (SEM, SU3500, Hitachi, Japan) was used to characterize the surface morphology of the samples. Since wood is an insulator, a thin layer of Au was evaporated onto the sample surface to eliminate charging using a sputtering device (Quorum SC7620, UK). Transmission electron microscopy (TEM, Talos F200X, FEI, USA) was performed to characterize the shape, size, and crystallinity of the nanocrystals with an accelerating voltage of 200 kV. Energy-dispersive X-ray spectrometry (EDS, INCA ACT250, Oxford Instruments, UK) operated at 30 mA and X-ray photoelectron spectroscopy (XPS, AXIS UltraDLD, Shimadzu, Japan) at high resolution scans with monochromatic Al-Kα X-ray source were employed to character the surface chemistry of the samples. The phase of the samples was determined by X-ray diffraction (XRD, XD-2, Beijing Purkinje General Instrument Co., Ltd., China) measurement using Cu Ka radiation at a scanning rate (2θ) of 8°/min in the degree range from 5° to 70°. Water contact angles and sliding contact angles measurements were performed on an OCA15 measuring system (DataPhysics Instruments GmbH, Germany) by using a water droplet of 4 uL. The sliding contact angles were obtained by calculating the difference between advancing and receding angle, which was measured by pumping and sucking water into and from the existing water droplet on the solid surface. The average of five measurements was reported as the final value.

3 Results and Discussion

3.1 Characterization of the as-prepared superhydrophobic surface

Superhydrophobic surface was effectively fabricated on wood substrate through assembly of hierarchical BiOCl and hydrophobic PFOTS layer (Figure 1). The need for complete immersion in solution guaranteed sufficient ethanol to be preserved inside the substrate. During this immersion process, enough BiOCl was also deposited on fiber surface. The liquid ethanol stored in substrate was transformed into gaseous ethanol with the assistance of heating treatment. The continuous release of gaseous ethanol had heavy impact force on BiOCl, which drove the assembly of hierarchical BiOCl. Simultaneously, PFOTS molecules reacted with hydroxyl groups from ethanol and thus generated hydrophobic layer. Wood, as a representative of lignocellulosic material, was used as substrate material to prepare self-healing superhydrophobic surface. The SEM, CA, EDS, XPS, XRD analysis were adopted to characterize the as-prepared samples.

Figure 2 shows surface morphology and wettability of the untreated and treated wood samples. Fence-like microscale protuberances with a smooth surface were observed on the untreated wood substrate (Figure 2a-b), indicating that wood has primary roughness, which is beneficial for fabrication of superhydrophobic structure. It can be found that fence-like protuberances were constituted of abundant fibers with a high length-diameter ratio (Figure 1b). The contact angle of wood surface was 69^{o}, presenting an intrinsic hydrophobicity. The EDS analysis shows that wood is composed of C and O element (Figure S1a, ESI). After coated with BiOCl, the wood

surface was covered with a continuous coating (Figure 2c). EDS spectra revealed that the top coating was rich in Bi and Cl element (Figure S1b, ESI), confirming the existence of BiOCl. The zoom in image revealed that dense BiOCl nanocrystals were deposited on wood surface without any convex or concave areas in support of micro-sized roughness (Figure 2d). As a result, the Bi-wood displayed a contact angle of 142^{o} and a sliding angle (SA) of above 90^{o}. TEM image shows that BiOCl nanocrystals had a size of about 50~100 nm with a square shape (Figure 2e). The HRTEM of a single nanoplate demonstrated clear lattice stripe, indicating the nanoplate with well-crystalized structure (Figure 2f). Moreover, the distance of lattice fringes was 0.27 nm, in accordance with the value of {110} plane of the tetragonal phase.

After coated with BiOCl and PFOTS, the sample achieved superhydrophobicity with a contact angle of 155^{o} and a sliding angle of 2^{o} (the inset in Figure 2g). SEM images show that Bi&F-wood was covered by hierarchical BiOCl coating with micro-sized grooves (Figure 2g-h). The appearance of F, Si indicated that hierarchical BiOCl was successfully modified by hydrophobic PFOTS. (Figure S1c, ESI). TEM image shows that BiOCl nanocrystals had almost no change in size and shape after PFOTS modification (Figure 2i). The clearly gray section in PFOTS modified BiOCl nanocrystals surface, similar to a shell layer, should be the production of the PFOTS after hydrolysis and condensation, which had been reported in previous literatures.[41-42] The HRTEM of an individual nanoplate also shows the clear lattice strip and the interplanar distance of 0.27 nm(Figure 2j), confirming that the crystal

type of BiOCl did not get affected by PFOTS modification.

Figure 3a shows the X-ray diffraction (XRD) patterns of the untreated sample, Bi-wood, Bi&F-wood. As shown in Figure 3a, strong diffraction peaks at 16^{o} and 22^{o} appeared in the three samples were attributed to the crystalline region of cellulose fiber, which is the main composition of lignocellulosic materials.[43] New diffraction peaks at 12^{o}, 24^{o},26^{o}, 32^{o}, 33.5^{o}, 37^{o}, 41^{o},47^{o}, 50^{o}, 54^{o}, 59^{o}, and 68^{o} related to 001, 002, 101, 110, 102 003, 112, 020, 004, 211, 122, and 220 were observed in Bi-wood and Bi&F-wood, corresponding to the tetragonal matlockite structure (JCPDF: 06-0249). The XRD pattern confirmed that the crystal type of BiOCl was not affected by PFOTS modification, consistent with TEM analysis. As a result, it can be verified that BiOCl crystals remained its inherent nature after hydrophobic modification, which is beneficial for imparting superhydrophobic surface with efficient photocatalytic ability.

Figure 3b-f show X-ray photoelectron spectroscopy (XPS) spectra of superhydrophobic coating The XPS spectra were revised for samples via referencing the C 1s peak at 248.5 eV. As shown in Figure 3b, the superhydrophobic coating exhibited the presence of C, O, Si, F, Bi, and Cl element. The BiOCl nanocrystals provided the major element for Bi, O, and Cl. The hydrophobic PFOTS layer, grafted onto BiOCl surface, offered the C, O, Si, and F element. The Bi 4f XPS spectrum shows two main peaks with binding energies at 159.4 eV and 164.8 eV (Figure 3c), corresponding to Bi $4f_{7/2}$ and Bi $4f_{2/5}$ of Be^{3+} , respectively. The peaks at 530.2 eV and 532.8 eV observed in O 1s XPS spectrum belonged to bismuth-oxygen bond in BiOCl

and surface hydroxyl (Figure 3d).[44] The slitting peaks of Cl 2p centered at 198.1 eV and 199.7 eV were separately related to Cl $2p^{3/2}$ and Cl $2p_{1/2}$ (Figure 3e), confirming the Cl- in BiOCl.[45] The F 1s XPS spectrum could be fitted well with the peak at 687.6 eV, which was attributed to $–CF_2$ groups from the PFOTS layer (Figure 3f).[13] The XPS analysis confirmed that the superhydrophobic coating was composed of hydrophobic PFOTS layer and BiOCl nanaocrystals.

3.2 Restoration of superhydrophobicity upon various severe damages

The as-prepared self-healing superhydrophobic surface can restore the superhydrophobicity of the area after various damages, even severe damages with deep and wide scratches. A series of harsh physical and chemical damages were employed to destroy the superhydrophobic surface and then to evaluate its self-healing capability. First, sandpaper abrasion was used to make the surface hydrophobic according to the analogical procedures described previously.[46] Specifically, the superhydrophobic surface was rubbed by a piece of sandpaper (1500 mesh) under 10 kPa pressure over a distance of 100 cm. The resultant surface became hydrophobic with a CA of ~123^o and an SA of larger than 90^o. The remarkably decreased contact angle and strong water adhesion resulted from the loss of hydrophobic PFOTS layer and the damaged hierarchical structure caused by severe sandpaper abrasion. A trace amount of coating separated from the sample and left on sandpaper also confirmed the serious damage (Figure S2, ESI). However, after heating at 150^{o}C for 15 min, the damaged surface recovered its superhydrophobicity with a CA of larger than 150^o. The damage-healing process can be repeated for more

than 9 times (Figure 4a), indicating an excellent self-healing capability.

During the healing process, it was found that the healing time significantly affected the degree of recovery of water repellency (Figure 4b). It took 15 min to restore the damaged surface from hydrophobicity (CA=123^{o}) to superhydrophobicity (CA>150^{o}) at 150^{o}C. However, the fully recovery of its original superhydrophobicity (CA=153^{o}) needed 20 min. As the heating time further prolongs, the resultant surface had a CA of larger than its original value, due to the accumulation of hydrophobic PFOTS molecules on the damaged surface. It can be found that CA value of the surface could reach 157^{o} within 30 min. Figure 4c shows the recovery time gradually increased with the increase of damage-healing cycles for 150^{o}C. The recovery time was prolonged to 55 min at 9th cycle. However, it can be accelerated by higher temperature. It took only 1 min to recover the superhydrophobicity at 9th cycle for 300 ^{o}C, which is one in 55 times spent at 150^{o}C. Consequently, the self-healing ability has strong relationship to the heating temperature. It is expected that the healing performance can be enhanced via tuning the heating temperature. As shown in Figure 4c, with the increase of heating temperature, the healing efficiency was improved, demonstrated by the need for less recovery time at the same damage-healing cycle. Moreover, higher temperature was beneficial for the stability of healing efficiency. It can be found that more recovery time was needed with the increase of damage-healing cycles for 100^{o}C, 150^{o}C, and 200^{o}C, while the need for recovery time kept almost constant for 250^{o}C, 300^{o}C. Additionally, the number of damage-healing cycles was also affected by heating temperature. The value of damage-healing cycles

was 4, 9, 13, 31, and 16 for 100^{o}C, 150^{o}C, 200^{o}C, 250^{o}C, and 300^{o}C, respectively. This demonstrated an increase tendency with the increase of heating temperature (within 250^{o}C). Also, the number of damage-healing cycles could be improved by increasing the amount of PFOTS (Figure S3, ESI). As a result, it could be confirmed that self-healing performance highly depends on the heating temperature.

Second, for further evaluation of self-healing behavior, wide and deep cuts penetrating to the underlying substrate were made according to previously reported method.[29] As shown in Figure 4d, a noticeable gap with about 100 um wide was exposed on the substrate after cutting. The magnified image shows the superhydrophobic coating was almost completely removed in the cut area (Figure 4e), which resulted in a high water adhesion on the damaged surface. It can be found that water droplet tightly adhered to the damage area even turning the sample upside down (inset in Figure 4d). Moreover, the disappearance of F, Si, Cl, and Bi element in the scratched area further confirmed the complete removal of BiOCl nanocrystals and the PFOTS layer (Table S1-2, ESI). After heating by a torch for 1s, the scratched area rapidly recovered the superhydrophobicity with an SA of ~0^{o} (the inset in Figure 4f). As shown in Figure 4f, the scratched area was significantly narrowed after heating treatment. The magnified SEM image shows that some neighbor undamaged fibers with superhydrophobic coating migrated to the naked area and recovered it (Figure 4g), mimicking the recovery mechanism of human skin.[28-29] EDS analysis demonstrated that the disappeared elements including F Si, Cl, and Bi reappeared on the healed area (Table S3, ESI), indicating the successful transfer of BiOCl and

PFOTS with the assistance of the migration of fiber.

Third, the self-repairing property towards other types of common destructions was also studied. As anticipated, the self-healing surface could recover the superhydrophobicity after damaged by various manners, including plasma etching, oil contamination, sun bleaching, ultrasonic vibration, water spray impact, and chemical corrosion (Figure S4, ESI). Based on the above-mentioned results, it can be verified that the as-prepared superhydrophobic surface achieved all-damage-healable ability.

The mechanism for the high restoration of diverse damages was illustrated in Figure 5. All the types of damages transform the surface from superhydrophobicity to hydrophobicity even to hydrophilicity via either decomposing the hydrophobic layer or destroying the elaborate structure. The removal of the hydrophobic layer on the outmost surface of the superhydrophobic sample leads to energy gap between interior and outer surface.[47] Meanwhile, energy gap was built between the damaged area and the undamaged area. When activated by thermal treatment, the PFOTS molecules with enough mobile energy can break up the energy gap and migrate to the damaged surface. The migration process can be accelerated by high temperatures. PFOTS molecules readily reacted with hydroxyl groups of residue ethanol and then regenerated a new hydrophobic PFOTS layer. The primary pores from substrate and abundant “air pockets” from hierarchical BiOCl&PFOTS coating provided enough space to store sufficient healing agents by means of physical absorption or chemical grafting. Therefore, the loss of the top low surface energy layer can be restored through the storage and release of healing agents (Figure 5a). The damaged

hierarchical structure caused by sandpaper abrasion, knife scratches and etc. can be repaired through the migration of fiber activated by thermal treatment. Specifically, wood is mainly constituted from fiber. When wood moisture is below fiber saturation point, the volume of wood will shrink with the decrease of moisture content. And, the big difference between longitudinal shrinkage and transverse shrinkage produces tensile stress, which drives the movement of fiber (such as warping). Thermal treatment results in the change in wood moisture, which arouses the response of fiber. Benefiting from the thermally responsive behavior, the fibers moved to the damaged area to and filled the gap once activated by heating process. Because of the strong adhesion between the superhydrophobic coating and the fibers, the coating can be transferred to the damaged/naked area from the neighbor undamaged area (Figure 5b-c). The synergistic self-healing mechanism facilitates the superhydrophobic lignocellulosic materials to restore both the hierarchical structure and the hydrophobic layer.

3.3 Bonding strength between the superhydrophobic coating and the substrate

The strong adhesion between the superhydrophobic coating and the substrate not only serves as the first barrier to resist mechanical wear, but also ensures the successful migration of the coating along with the movement of fiber. Here, a series of physical wear tests were carried out to evaluate the bonding strength between the coating and the substrate. First, adhesive tape was used to destroy the superhydrophobic coating. As shown in Figure S5, after tightly glued by adhesive tape and then rapidly peeled it off, the resulting surface could still support spherical water

droplets. Second, as a standard wear test, sandpaper abrasion was employed for further evaluation. Figure S6 shows the methodology in detail. Silicon carbide sandpaper (1500 mesh) served as abradant material, whereas superhydrophobic surface was faced to the sandpaper and pushed in one direction at a pressure of 1.2 kPa, 2.6kPa, and 5 kPa, respectively. The CAs and SAs of the resulting surface were recorded every 10 cm of abrasion length. Figure 6a-b show that the resultant surface retained supehydrophobicity with a CA larger than 150^{o} and an SA below 10^{o} even after being abraded over 120 cm abrasion length at the pressure of 1.2 kPa, over 100 cm abrasion length at the pressure of 2.6 kPa, and over 60 cm abrasion length at the pressure of 5 kPa, respectively, indicating strong substrate adhesion of the superhydrophobic coating.

Similar abrasion test was also performed using 800 mesh sandpaper at the pressure of 2.6 kPa. In the first abrasion length of 10 cm, the resultant surface remained superhydrophobic even though its CA was decreased. When the abrasion length was increased to 20 cm, the target surface lost superhydrophobicity with a CA of ~145^{o} and an an SA lager than 90^{o}. However, the damaged surface fully recovered its superhydrophobicity with a CA of ~153^{o} and an SA of ~6^{o} after heated by a butane torch for 1 s. Evidently, the healing process was convenient and efficient. With the support of self-healing ability, the maximum affordable abrasion length could be extended to 800 cm (Figure 6c), indicating enhanced mechanical robustness. Therefore, it can be concluded that self-healing behavior serves as second barrier to resist mechanical destructions.

The above-mentioned results provided solid proof for the strong adhesion between superhydrophobic coating and the substrate.

3.4 Tunable and stable photocatalytic degradation of organic pollutants.

Imparting superhydrophobic materials with photocatalytic function is an effective approach to enhancing their resistance towards organic contamination. To explore the photocatalytic ability of the as-prepared samples, decomposition of organic pollutant (RhB) under an ambient condition was conducted. The typical absorption peak at 554 nm was used to monitor the degradation process.

Degradation efficiency of the as-prepared samples: Figure 7a-c show the temporal evolution of the UV-vis spectrum of the RhB solution degraded by three catalytic samples. These samples included the untreated wood, Bi-wood and Bi&F-wood. It can be observed from Figure 7a that the intensity of absorption spectra of the RhB solution, degraded by the untreated wood, was decreased but still observable for 80 min. Figure 7b-c show that the intensity of the absorption spectra of RhB solutions, respectively degraded by Bi-wood and Bi&F-wood in the dark, had negligible change. However, the absorption peak of RhB solutions was almost completely disappeared when catalyzed by Bi-wood and Bi&F-wood under UV irradiation for 80 min (Figure 7d-e).

Figure 7f shows the change in RhB concentrations (C/C_0) with different photocatalytic samples over time. The untreated wood demonstrated high physical absorption with a dye absorption efficiency of 80% after 80 min (Figure $7f_1$). However, even prolong the immersion time, the RhB concentration could not be

further reduced. After wood coated with hydrophobic BiOCl or BiOCl&PFOTS coating, its physical absorption behavior was dramatically impaired. As shown in Figure 7, the absorption efficiency was decreased to 38% for Bi-wood and 20% for Bi&F-wood (Figure 7f_2-f_3), which was attributed to their enhanced water repellency. Figure 7f_4-f_5 show the photocatalytic degradation efficiency of the Bi-wood and the Bi&F-wood under UV light irradiation. The photocatalytic degradation efficiency was 90% for the Bi-wood, while it was 100% for the Bi&F-wood after 80 min UV irradiation. Because of the ignorable physical absorption ability of the two samples, their excellent degradation performance was mainly ascribed to the photocatalytic effect from BiOCl nanocrystals.

In particular, it was worthy to note that the Bi&F-wood coated with BiOCl&PFOTS composite showed higher photocatalytic activity compared with that of the Bi-wood coated with pure BiOCl. The photocatalycity enhanced mechanism was schematically shown in Figure 8. The BiOCl&PFOTS coating demonstrated superhydrophobic surface while the BiOCl coating failed to achieve extreme water repellency. Superhydrophobicity helps the Bi&F-wood to rapidly separate RhB molecules from RhB aqueous solution by tuning the absorption competition between water and RhB molecules,[48] which could effectively improve RhB concentration around active sites. Without separation function, Bi-wood possessed poor absorption towards RhB molecules owing to the occupation of water on active sites. Moreover, owing to the existence of hierarchical structure, the BiOCl&PFOTS coating has higher surface area compared with that of BiOCl coating. It has been reported that

large surface area is in favor of the accumulation of RhB molecules around active photocatalytic sites.[49-50] High concentration of pollutants on photocatalyst can enhance the photocatalytic activity.[51] As a result, Bi&F-wood demonstrated better photocatalytic performance within a limited UV irradiation time. The change in CA of these two samples before and after degrading RhB solution was also different, which has been discussed in detail in part of "Electronic Supplementary Information" (Figure S7, ESI). Based on the above-mentioned results and analysis, we suspect that photocatalytic performance may be able to be controlled by tuning surface wettability, which will be further studied in our future work.

Stability and reusability of the as-prepared sample: The stability and reusability of the photocatalytic Bi&F-wood were studied using cyclic degradation tests. The catalytic reaction time was set to be 80 min. 14 cycles were conducted in total and corresponding photocatalytic activity was shown in Figure 7g. The change in CAs of the resulting sample at each cycle was also recorded. As shown in Figure 7g, the photocatalytic degradation efficiency could reach 100% within 6 cycles. Meanwhile, the Bi&F-wood remained superhydrophobicity with CAs of ~150^{o} and SAs of ~10^{o} (Figure S8, ESI). Therefore, the as-prepared superhydrophobic coating simultaneously possessed stable superhydrophobicity and photocatalytic activity, which has been rarely reported. This is because that it is difficult for UV light to break the long chain of C-F bond from PFOTS and thus prevents the damage of hydrophobic layer after long time UV irradiation.[52] Moreover, before the next catalytic cycle, Bi&F-wood was taken out from RhB solution, washed with water, and

then dried in a drying oven. Hence, even though the hydrophobic PFOTS layer was decomposed, a new one could be regenerated in support of superhydrophobicity through the self-healing mechanism (i.e., migration of PFOTS). Additionally, BiOCl nanocrystals were tightly anchored by the polymer from PFOTS, which avoids BiOCl solids to be separated from substrate during magnetic stirring and thus minimizes the wastage of photocatalyst after each degradation cycle. It has also been reported that suprhydrophobicity could protect photocatalysts from hydrolytic degradation, which contributes to more reliable photocatalytic performance.[53] As a result, Bi&F-wood simultaneously exhibited superhydrophobicity and desirable photocatalytic activity. The Bi&F-wood lost superhydrophobicity after 6^{th} cycle. However, the degradation efficiency was still beyond 97% in subsequent test, confirming the excellent stability reusability of Bi&F-wood as photocatalyst.

4. Conclusion

In summary, we demonstrated a kind of all-damage healable superhydrophobic surface with photocatalytic activity through assembly of hierarchical BiOCl and hydrophobic PFOTS layer on wood substrate. In contrast to most traditional self-healing surfaces, the as-prepared superhydrophobic surface could restore wide and deep cuts via healability conveyance method. Specifically, fibers, as the main constitution of lignocellulosic materials such as wood, have an intrinsic thermal responsive property. By a simple heating treatment, the fibers could convey the superhydrophobic coating into the damage area. In this way, the cuts were narrowed or filled and thus regenerated superhydrophobicity. As far as we know, this is the first

report on fabrication of healable superhydrophobic surface capable of repairing rigorously damaged hierarchical structure by using the substrate materials' intrinsic property. Moreover, BiOCl nanocrystals were introduced into the superhydrophobic coating, which imparted the superhydrophobic surface with photocatalaticity. Taken photocatalytic degradation of RhB as an example, the superhydrophobic coating could degrade RhB aqueous solution for 14 times without compromising photocatalytic efficiency, demonstrating remarkable stability and reusability. Interestingly, it was found that the photocatalytic activity was dependent on surface wettability. For example, the BiOCl&PFOTS coating with superhydrophobic surface presented higher photocatalytic activity compared with that of BiOCl coating with hydrophobic surface. The obtained self-healing superhydrophobic surface with photocatalytic property should inspire the development of multifunctional intelligent materials for applications in related fields.

Acknowledgements

This work was financially supported by the National Natural Science Foundation of China (31870552)，the Major Science and Technology Program of Hunan Province (2017NK1010), Young Elite Scientists Sponsorship Program by CAST (2016QNRC001), Outstanding Innovative Youth Training Program of Changsha (KQ1707019), Hunan Provincial Technical Innovation Platform and Talent Program in Science and Technology (2016RS2010, 2016TP1013), and Science and Technology Innovation Fund for Graduate Students, from Central South University of Forestry and Technology (20181013). S.J. thanks for the funding from China Scholarship

Council (CSC). Y. Lu acknowledges the support from EPSRC project EP/N024915/1.

References

1.Y. Xiong, C. Wang, H.W. Wang, Q.F. Yao, B.T. Fan, Y.P. Chen, Q.F. Sun, C.D. Jin, X. Xu, A 3D titanate aerogel with cellulose as the adsorption-aggregator for highly efficient water purification, J. Mater. Chem. A 5 (2017) 5813-5819.

2. D. Klemm, B. Heublein, H.P. Fink, A. Bohn, Cellulose: fascinating biopolymer and sustainable raw material, Angew. Chem. 44 (2005) 3358-3393.

3. S.H. Li, S.B. Zhang, X.H. Zhang, Fabrication of superhydrophobic cellulose-based materials through a solution-immersion process, Langmuir 24 (2008) 5585-5590.

4. C.J. Zhou, Y.L. Wu, T.Z. Lei, I.I. Negulescu, Adsorption kinetic and equilibrium studies for methylene blue dye by partially hydrolyzed polyacrylamide/cellulose nanocrystal nanocomposite hydrogels, Chem. Eng. J. 251 (2014) 17-24.

5. Y. Xiong, C. Wang, H.W. Wang, C.D. Jin, Q.F. Sun, X. Xu, Nano-cellulose hydrogel coated flexible titanate-bismuth oxide membrane for trinity synergistic treatment of super-intricate anion/cation/oily-water, Chem. Eng. J. 337 (2018) 143-151.

6. Y.Q. Wu, S.S. Jia, Y. Qing, S. Luo, M. Liu, A versatile and efficient method to fabricate durable superhydrophobic surfaces on wood, lignocellulosic fiber, glass, and metal substrates, J. Mater. Chem. A 4 (2016) 14111-14121.

7. H.Z. Guo, P. Fuchs, K. Casdorff, B. Michen, M. Chanana, H. Hagendorfer, E.R. Yaroslav, Bio-inspired superhydrophobic and omniphobic wood surfaces, Adv. Mater. Interfaces 4 (2017) 1600289.

8. D.W. Zhao, C.J. Chen, Q. Zhang, W.S. Chen, S.X. Liu, Q.W. Wang, Y.X. Liu, J. Li, H.P. Yu, Solid-state supercapacitors based on a renewable and biodegradable mesoporous cellulose membrane, Adv. Energy Mater. 7 (2017) 605-610.

9. C.H. Xue, Y.R. Li, P. Zhang, J.Z. Ma, S.T. Jia, Washable and wear-resistant superhydrophobic surfaces with self-cleaning property by chemical etching of fibers and hydrophobization, ACS. Appl. Mater. Interfaces 6 (2014) 10153-10161.

10. D.W. Zhao, Q. Zhang, W.S. Chen, X. Yi, S.X. Liu, Q.W. Wang, Y.X. Liu, J. Li, X.F. Li, H.P. Yu, Highly flexible and conductive cellulose-mediated PEDOT: PSS/MWCNT composite films for supercapacitor electrodes, ACS. Appl. Mater. Interfaces 9 (2017) 13213-13222.

11. S. Lee, B. Kim, S.H. Kim, E. Kim, J.H. Jang, Superhydrophobic, reversibly elastic, moldable, and electrospun (SupREME) fibers with multimodal functions: from oil absorbents to local drug delivery adjuvants, Adv. Funct. Mater. 27 (2017) 1702310.

12. P. Khanjani, A.W.T. King, G.J. Partl, L.S. Johansson, M.A. Kostiainen, R.H.A. Ras, Superhydrophobic paper from nanostructured fluorinated cellulose esters, ACS. Appl. Mater. Interfaces 10 (2018) 11280-11288.

13. Y. Lu, S. Sathasivam, J.L. Song, C.R. Crick, C.J. Carmalt, I.P. Parkin, Robust self-cleaning surfaces that function when exposed to either air or oil 347 (2015) 1132-1135.

14. B.T. Guo, Y.Z. Liu, Q. Zhang, F.Q. Wang, Q.W. Wang, Y.X. Liu, J. Li, H.P. Yu, Efficient flame-retardant and smoke-suppression properties of Mg-Al-ayered

double-hydroxide nanostructures on wood substrate, ACS. Appl. Mater. Interfaces 9 (2017) 23039-23047.

15. Y.Q. Wu, S.S. Jia, S. Wang, Y. Qing, N. Yan, Q.H. Wang, T.T. Meng, A facile and novel emulsion for efficient and convenient fabrication of durable superhydrophobic materials, Chem. Eng. J. 328 (2017) 186-196.

16. Y.S. Li, H. Shao, P.F. Lv, C.Y. Tang, Z.K. He, Y.L. Zhou, M.B. Shuai, J. Mei, W.M. Lau, Fast preparation of mechanically stable superhydrophobic surface by UV cross-linking of coating onto oxygen-inhibited layer of substrate, Chem. Eng. J. 338 (2018) 440-449.

17. X.L. Tian, T. Verho, R.H.A. Ras, Moving superhydrophobic surfaces toward real-world applications, Science, 352 (2016) 142-143.

18. X.J. Guo, C.H. Xue, S.T. Jia, J.Z. Ma, Mechanically durable superamphiphobic surfaces via synergistic hydrophobization and fluorination, Chem. Eng. J. 320 (2017) 330-341.

19. Y. Li, S.S. Chen, M.C. Wu, J.Q. Sun, All spraying processes for the fabrication of robust, self-healing, superhydrophobic coatings, Adv. Mater. 26 (2014) 3344-3348.

20. X. Zhang, Y.F. Si, J.L. Mo, Z.G. Guo, Robust micro-nanoscale flowerlike ZnO/epoxy resin superhydrophobic coating with rapid healing ability, Chem. Eng. J. 313 (2017) 1152-1159.

21. H. Zhang, Y. Ma, J.J. Tan, X.L. Fan, Y.B. Liu, J.W. Gu, B.L. Zhang, H.P. Zhang, Q.Y. Zhang, Robust, self-healing, superhydrophobic coatings highlighted by a novel branched thiol-ene fluorinated siloxane nanocomposites, Compos. Sci. Technol. 137

(2016) 78-86.

22.H. Zhou, H.X. Wang, H.T. Niu, Y. Zhao, Z.G. Xu, T. Lin, A waterborne coating system for preparing robust, self-healing, superamphiphobic surface, Adv. Funct. Mater. 27 (2017) 11280-11288.

23. K.L. Chen, S.X. Zhou, S. Yang, L.M. Wu, Fabrication of all-water-based self-repairing superhydrophobic coatings based on UV-responsive microcapsules, Adv. Funct. Mater. 25 (2015) 1035-1041.

24. X.C. Tian, S. Shaw, K.R. Lind, L. Cademartiri, Thermal processing of silicones for green, scalable, and healable superhydrophobic coatings, Adv. Mater. 28 (2016) 3677-3682.

25. H. Zhang, C.P. Hou, L.X. Song, Y. Ma, Z. Ali, J.W. Gu, B.L. Zhang, H.P. Zhang, Q.Y. Zhang, A stable 3D sol-gel network with dangling fluoroalkyl chains and rapid self-healing ability as a long-lived superhydrophobic fabric coating, Chem. Eng. J. 334 (2018) 598-610.

26. L.M. Qin, N. Chen, X. Zhou, Q.M. Pan, A superhydrophobic aerogel with robust self-healability, J. Mater. Chem. A. 6 (2018) 4424-4431.

27. G.C. Gurtner, W. Sabine, B. Yann, T.L. Michael, Wound repair and regeneration, Nature 453 (2008) 314-321.

28. P. Martin, Wound healing--aiming for perfect skin regeneration, Science 276 (1997) 75-81.

29. M.C. Wu, Y. Li, N. An, J.Q. Sun, Applied voltage and near-infrared light enable healing of superhydrophobicity loss caused by severe scratches in conductive

superhydrophobic films, Adv. Funct. Mater. 26 (2016) 6777-6784.

30. T. Kamegawa, Y. Shimizu, H. Yamashita, Superhydrophobic surfaces with photocatalytic self-cleaning properties by nanocomposite coating of TiO_2 and polytetrafluoroethylene, Adv. Mater. 24 (2012) 3697-3700.

31. W.S.Y. Wong, G.Y. Liu, A. Tricoli, Superamphiphobic bionic proboscis for contamination-free manipulation of nano and core-shell droplets, Small 13 (2017) 1603688.

32. C.M. Sheng, C. Wang, H.W. Wang, C.D. Jin, Q.F. Sun, S. Li, Self-photodegradation of formaldehyde under visible-light by solid wood modified via nanostructured Fe-Doped WO_3 accompanied with superior dimensional stability, J. Hazard. Mater. 328 (2017) 127-139.

33. Y. Xiong, C. Wang, H.W. Wang, C.D. Jin, Q.F. Sun, X.J. Xu, Endowing graphene with superior Cation/Anion Co-purification and visible photocataly sis performances by in situ deposition of silver compounds, J. Mater. Chem. A. 5 (2017) 20903-20910.

34. J.L. Liu, Y.H. Wang, J.Z. Ma, Y. Peng, A.Q. Wang, A review on bidirectional analogies between the photocatalysis and antibacterial properties of ZnO, J. Alloy. Compd. 783 (2018) 898-918.

35. Y. Ye, Z.G. Zang, T.W. Zhou, F. Dong, S.R. Lu, X.S. Tang, W. Wei, Y.B. Zhang, Theoretical and experimental investigation of highly photocatalytic performance of CuInZnS nanoporous structure for removing the NO gas, J. Catal. 357 (2018) 100-107.

36. M.Q. Wen, T. Xiong, Z.G. Zang, W. Wei, X.S. Tang, F. Dong, Synthesis of

MoS2/gC3 N4 nanocomposites with enhanced visible-light photocatalytic activity for the removal of nitric oxide (NO), Opt. express 24 (2016) 10205-10212.

37. Z.Y. Deng, W. Wang, L.H. Mao, C.F. Wang, S. Chen, Versatile superhydrophobic and photocatalytic films generated from TiO2–SiO2@PDMS and their applications on fabrics, J. Mater. Chem. A 2 (2014) 4178-4184.

38. L.Q. Ye, L. Zan, L.H. Tian, T.Y. Peng, J.J. Zhang, The {001} facets-dependent high photoactivity of BiOCl nanosheets, Chem. Commun. 47 (2011) 6951-6953.

39. X. Zhang, X.B. Wang, L.M. Wang, W.K. Wang, L.L. Long, W.W. Li, H.Q. Yu, Synthesis of a highly efficient BiOCl single-crystal nanodisk photocatalyst with exposing {001} facets, ACS. Appl. Mater. Interfaces 6 (2014) 7766-7772.

40. K. Zhang, J. Liang, S. Wang, J. Liu, K.X. Ren, X. Zheng, H. Luo, Y.J. Peng, X. Zou, X. Bo, J.H. Li, X.B. Yu, BiOCl sub-microcrystals induced by citric acid and their high photocatalytic activities, Cryst. Growth Des. 12 (2012) 793-803.

41. X. Deng, L. Mammen, H.J. Buttl, D. Vollmer, Candle soot as a template for a transparent robust superamphiphobic coating, Science 335 (2012) 67-70.

42. J.Y. Liang, L. Wang, J.X. Bao, L. He, Durable superhydrophobic/highly oleophobic coatings from multi-dome SiO_2 nanoparticles and fluoroacrylate block copolymers on flat substrates, J. Mater. Chem. A. 3 (2015) 20134-20144.

43. M. Saiful, S. Hamdana, I. Jusohb, M.R. Rahmana, A.S. Ahmed, The effect of alkali pretreatment on mechanical and morphological properties of tropical wood polymer composites, Mater. Design 33 (2012) 419-424.

44. Y.H. Shen, X. Yu, W.T. Lin, Y. Zhu, Y.M. Zhang, A facile preparation of

immobilized BiOCl nanosheets/TiO_2 arrays on FTO with enhanced photocatalytic activity and reusability, Appl. Surf. Sci. 399 (2017) 67-76.

45.Y. Li, Q. Wang, B. Liu, J. Zhang, The {001} facets-dependent superior photocatalytic activities of BiOCl nanosheets under visible light irradiation, Appl. Surf. Sci. 349 (2015) 957-969.

46. K.L. Chen, W.W. Gou, L. Xu, Y. Zhao, Low cost and facile preparation of robust multifunctional coatings with self-healing superhydrophobicity and high conductivity, Compos. Sci. Technol. 156 (2018) 177-185.

47. H.Y. Wang, Z.J. Liu, X.G. Zhang, C.J. Lv, R.X. Yuan, Y.J. Zhu, L.W. Mu, J.H. Zhu, Durable self-healing superhydrophobic coating with biomimic “chloroplast” analogous structure, Adv. Mater. Interfaces 3 (2016) 1600040.

48. A.H. Mamaghani, F. Haghighat, C.S. Lee, Photocatalytic oxidation technology for indoor environment air purification: the state-of-the-art, Appl. Catal. B: Environ. 203 (2017) 247-269.

49. S. Perni, C. Piccirillo, A. Kafizas, M. Uppal, J. Pratten, Antibacterial activity of light-activated silicone containing methylene blue and gold nanoparticles of different sizes, J. Clust. Sci. 21 (2010) 427-438.

50. C.R. Crick, J.C. Bear, A. Kafizas, I.P. Parkin, Superhydrophobic photocatalytic surfaces through direct incorporation of titania nanoparticles into a polymer matrix by aerosol assisted chemical vapor deposition, Adv. Mater. 24 (2012) 3505-3508.

51. A. Alonso-Tellez, R. Masson, D. Robert, N. Keller, V. Keller, Comparison of Hombikat UV100 and P25 TiO_2 performance in gas-phase photocatalyticoxidation

reactions, J. Photochem. Photobiol. A: Chem. 250 (2012) 58-65.

52.C.H. Xue, W. Yin, P. Zhang, J. Zhang, P.T. Jia, S.T. Jia, S.T. Jia, UV-durable superhydrophobic textiles with UV-shielding properties by introduction of ZnO/SiO_2 core/shell nanorods on PET fibers and hydrophobization, Colloids Surf. A. Physicochem. Eng. Asp. 427 (2013) 7-12.

53. Q. Sun, B. Aguila, G. Verma, X.L. Liu, Z.F. Dai, F. Deng, X.J. Meng, F.S. Xiao, S.Q. Ma, Superhydrophobicity: constructing homogeneous catalysts into superhydrophobic porous frameworks to protect them from hydrolytic degradation, Chem. 1 (2016) 628-639.

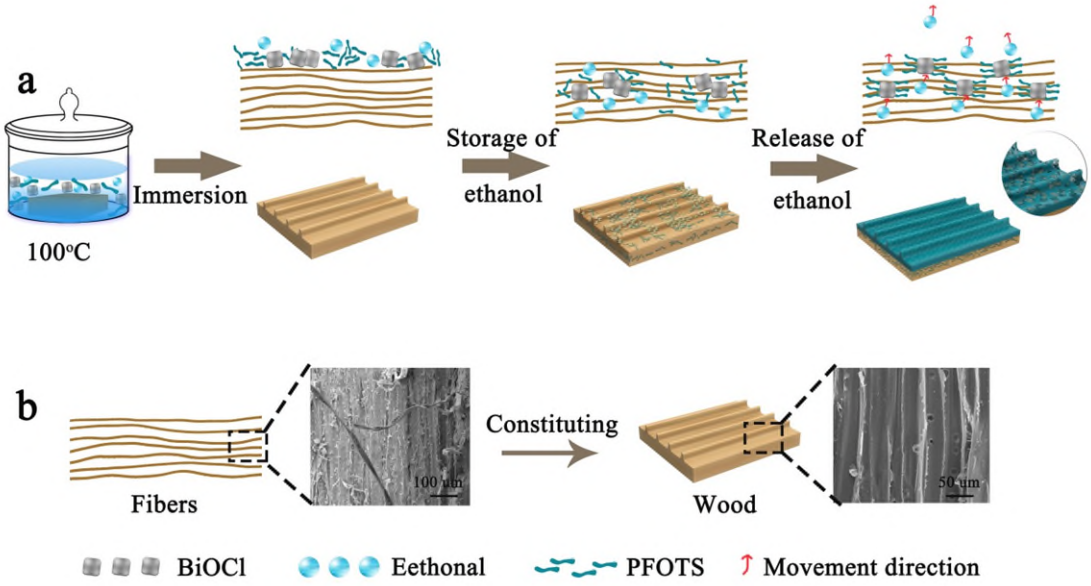

Revised-Figure 1 Schematic illustration of (a) the fabrication of self-healing superhydrophobic surface and (b) wood composition.

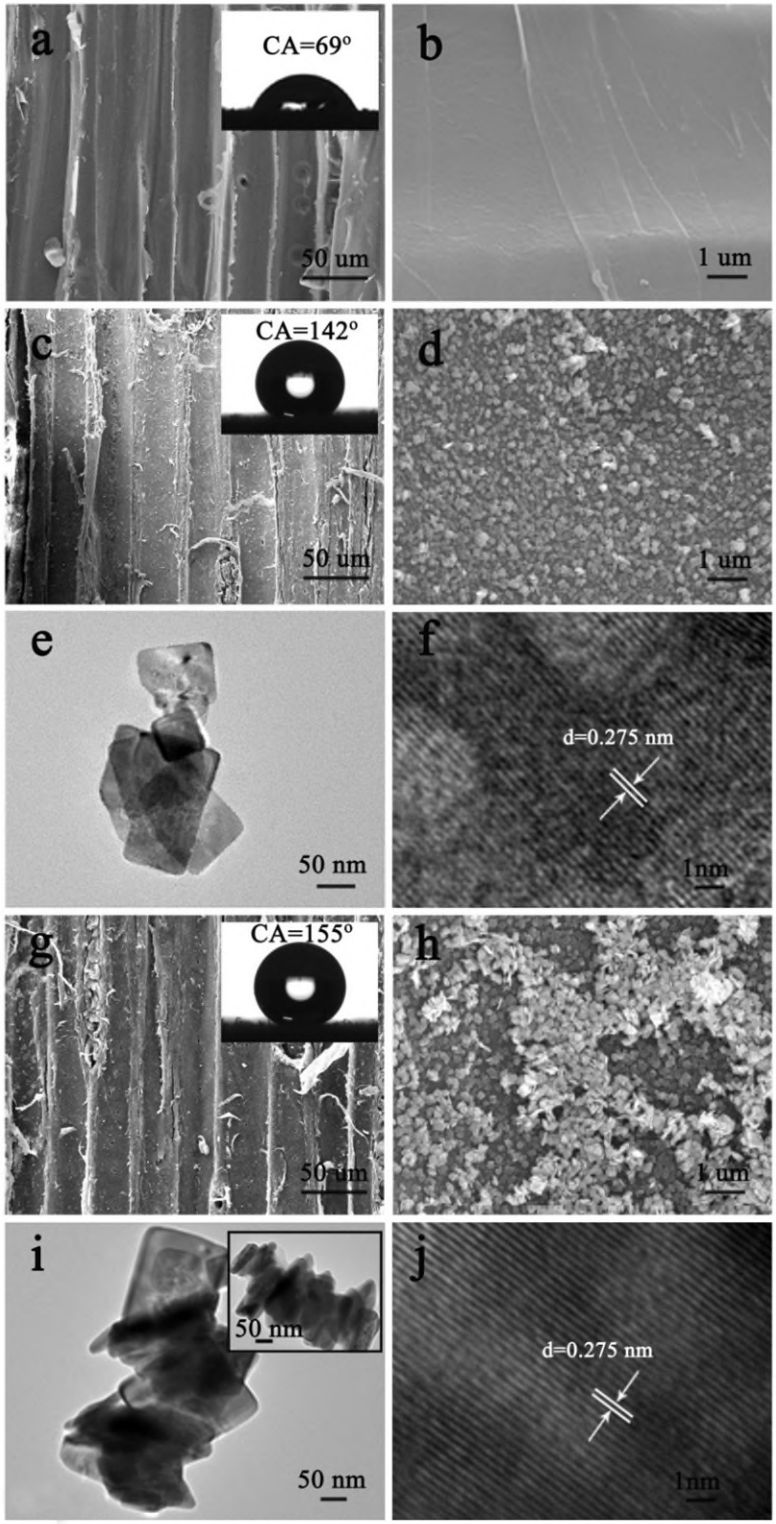

Figure 2 SEM images of the (a) untreated wood, (b) magnified image of (a), and (c) Bi-wood, (d) the magnified image of (c). (e) TEM image of BiOCl nanoplates. (f) HRTEM image of single BiOCl nanoplate. SEM images of the (g) Bi&F-wood, (h)

the magnified image of (g). (i) TEM image of BiOCl nanoplates modified by PFOTS. (f) HRTEM image of single BiOCl nanoplate after being modified by PFOTS.

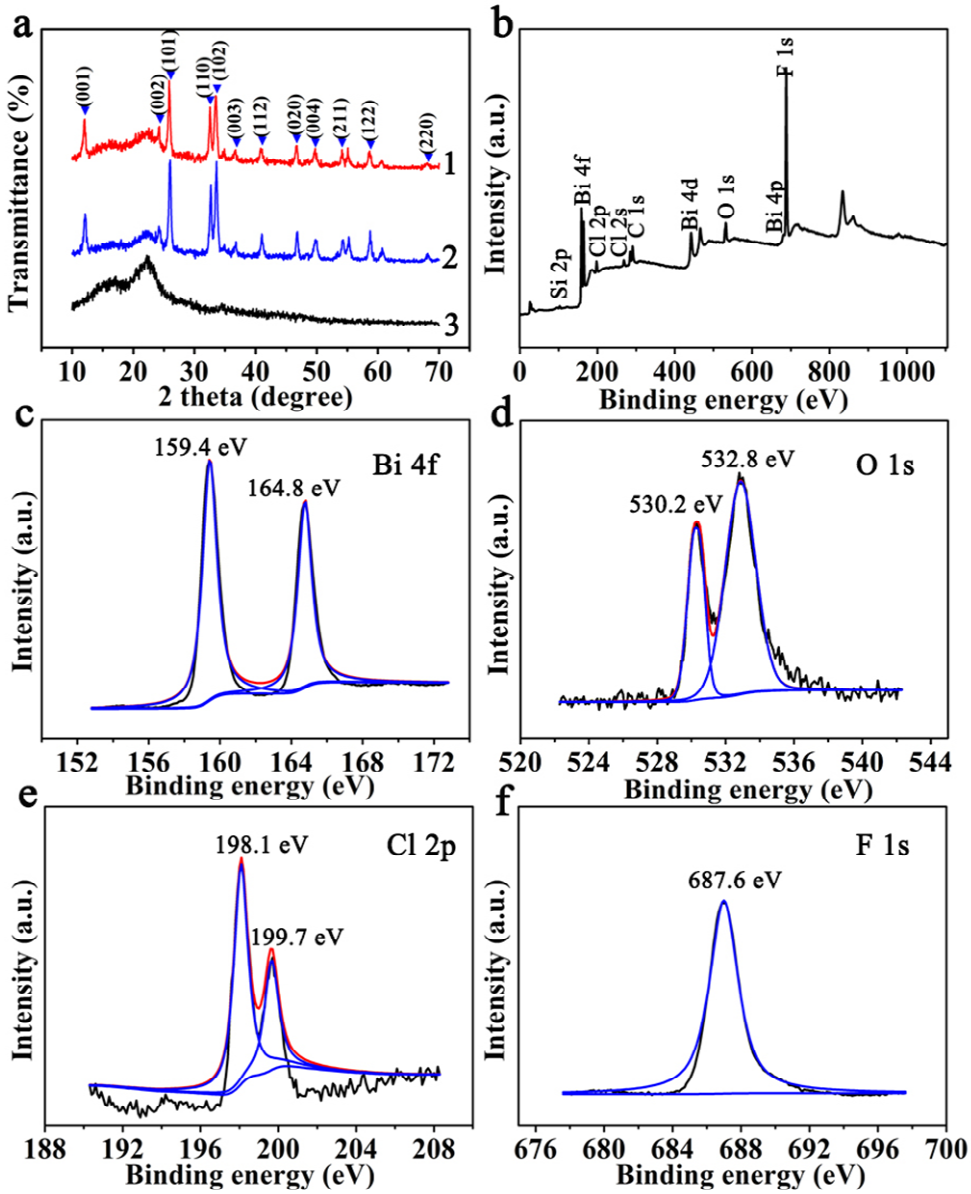

Figure 3 (a) XRD patterns of the (a_1) Bi&F-wood, (a_2) Bi-wood, and (a_3) untreated wood. (b) Survey-scan XPS spectra of PFOTS modified BiOCl, (c) Bi 4f, (d) O 1s and (e) Cl 2p for BiOCl-Y001 nanoplates, (f) F 1s for PFOTS.

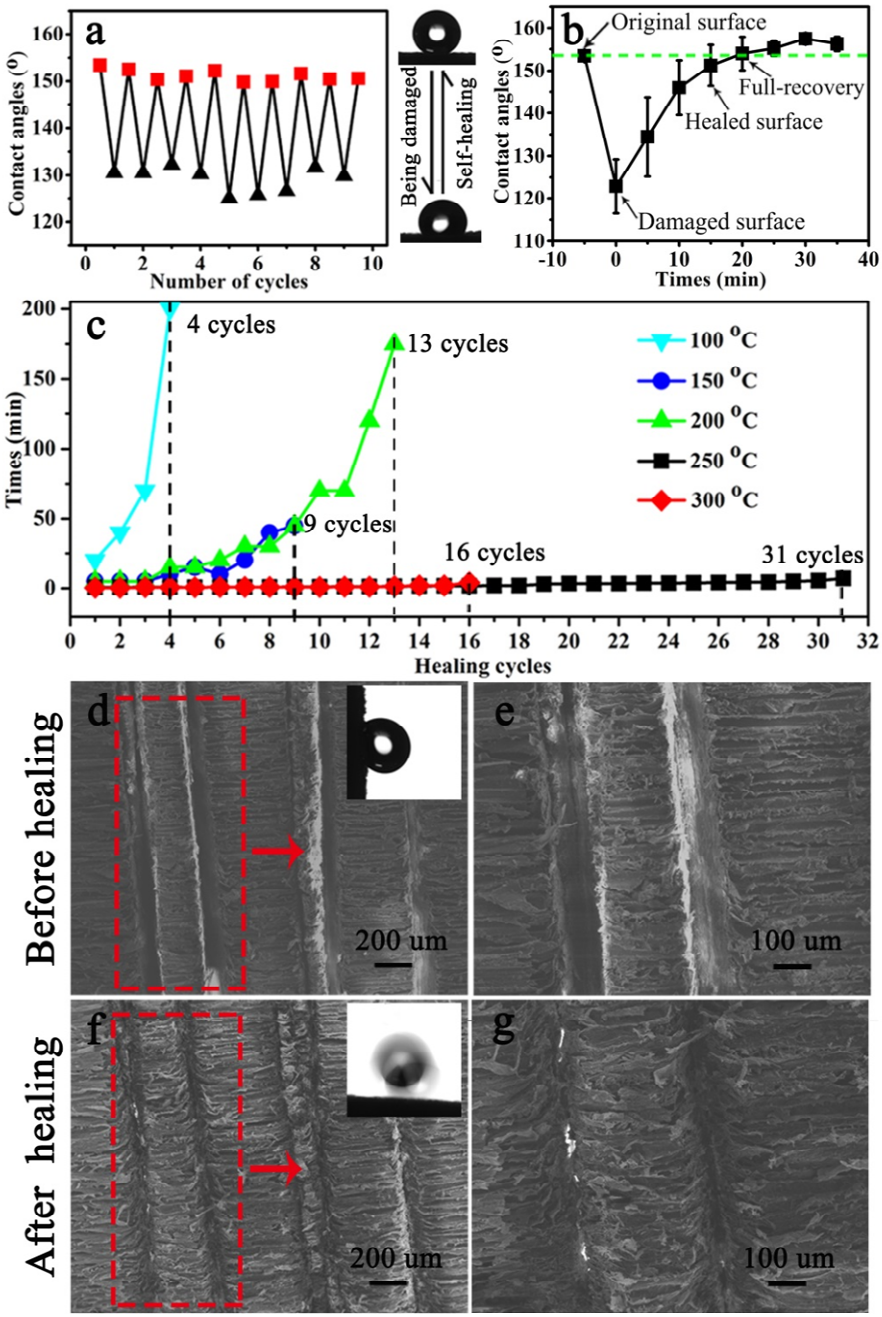

Figure 4 (a) Changes in the CA of the superhydrophobic sample before (▲) and after healing ( ). The rig of (a) is optical pictures of the as-prepared superhydrophobic sample after being damaged by sandpaper abrasion (bottom) and healed (top), respectively. (b) Changes in CA of the superhydrophobic sample during heating process (T=150 °C). (c) The changes in recovery time with increased

damaging/healing cycles at different temperatures. SEM images of the superhydrophobic sample with a ~100 um wide cut (d, e) before and (f, g) after being healed. Insets demonstrate the water adhesion behavior of the sample before and after healing.

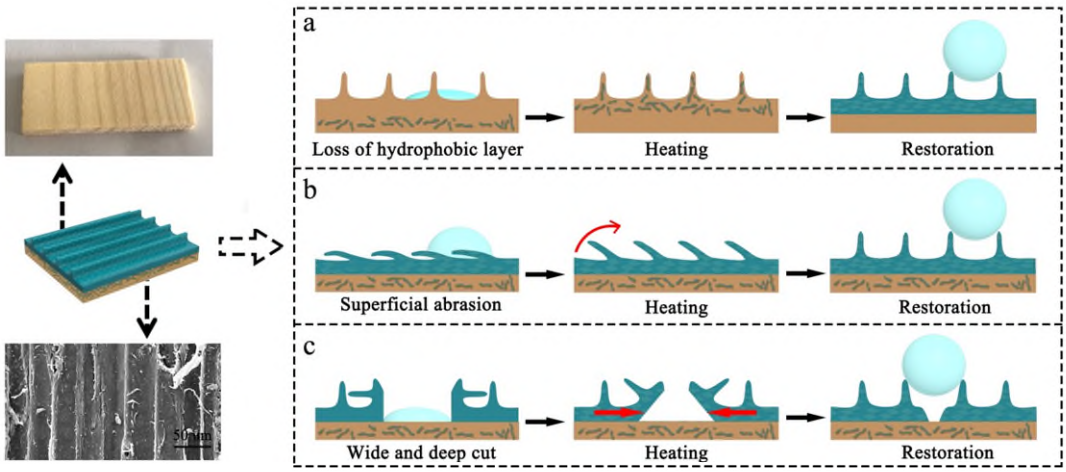

Figure 5 Schematic illustration of the healing behavior of the area after various damages.

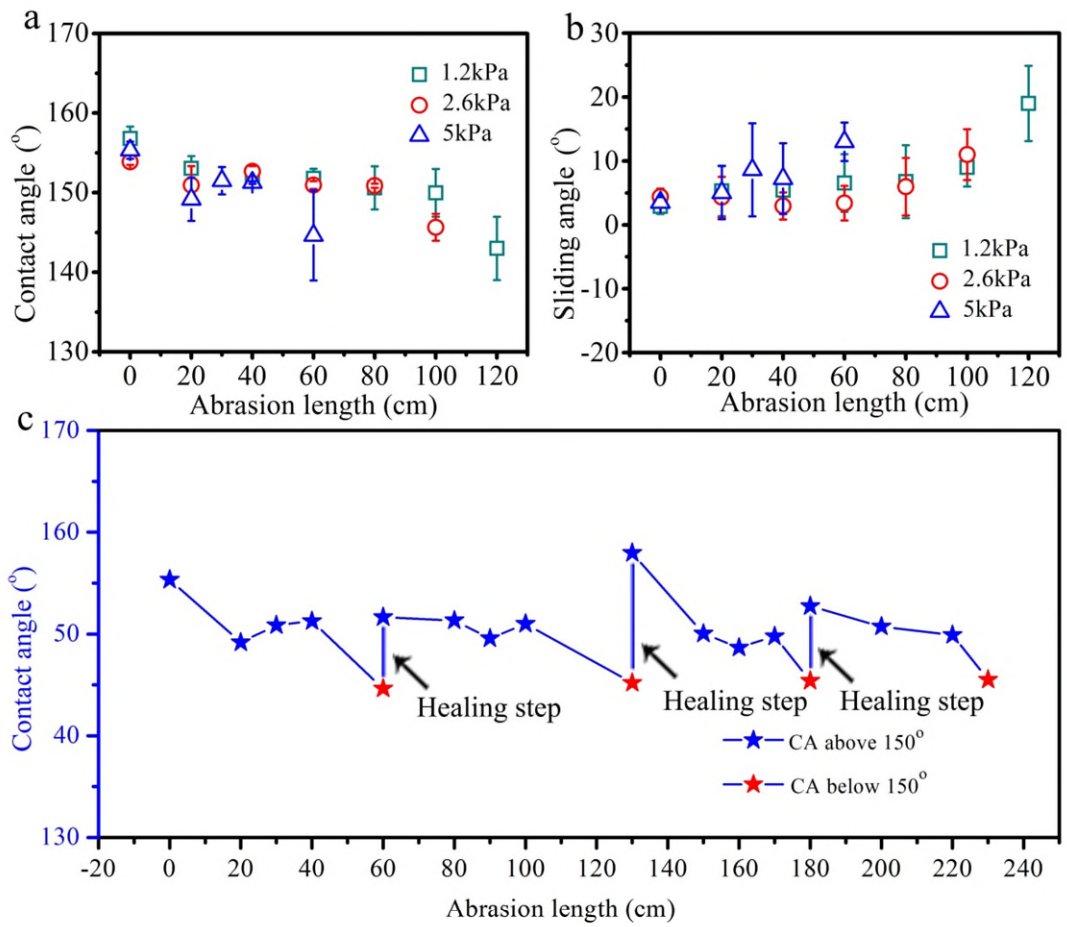

Revised-Figure 6 Abrasion length-dependent (a) CA and (b) SA of the resulting surface rubbed under different pressure using 1500 mesh sandpaper. (c) Superhydrophobic stability towards sandpaper abrasion (800 mesh, 2.6kPa) with support of self-healing ability.

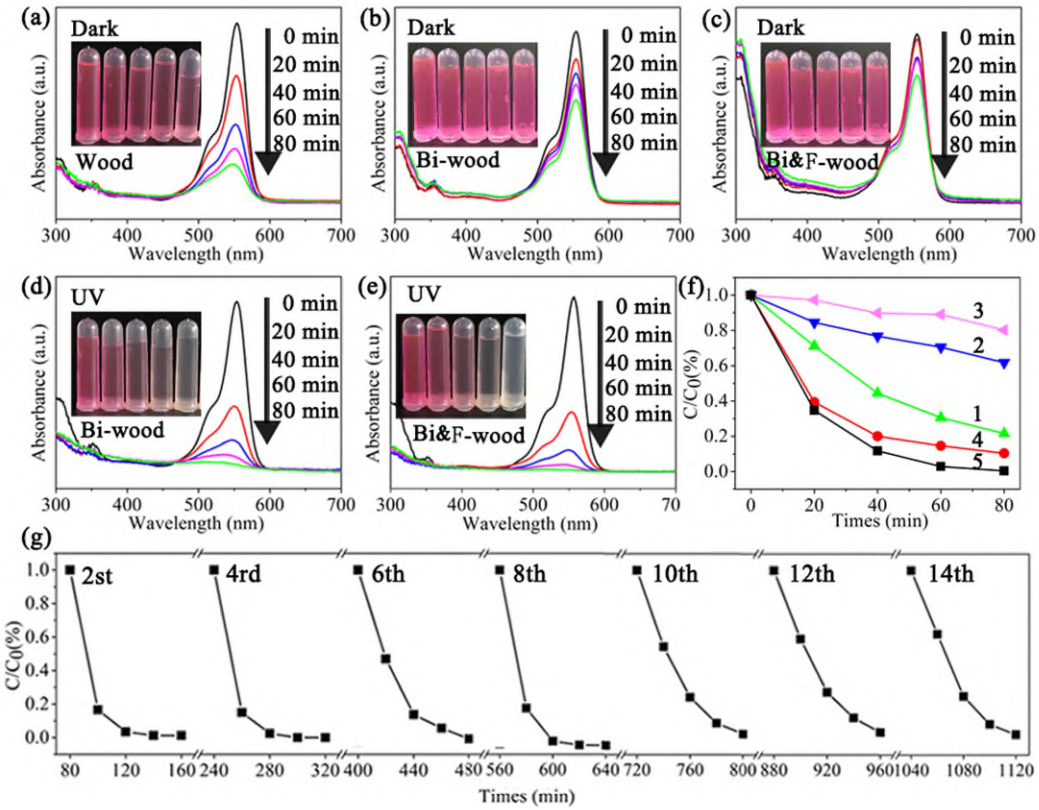

Figure 7 Photodecomposition of RhB with the (a) untreated wood, (b) Bi-wood, and (c) Bi&F-wood in the dark. Photodecomposition of RhB with the (d) Bi-wood and (e) Bi&F wood under UV irradiation. (f) Comparison of the degradation rate of RhB with different samples as photocatalysts in the dark or under UV irradiation and f_1-f_5 corresponding to a-e, respectively. (g) Cycling curves of photocatalytic degradation of RhB with Bi&F-wood as the photocatalyst.

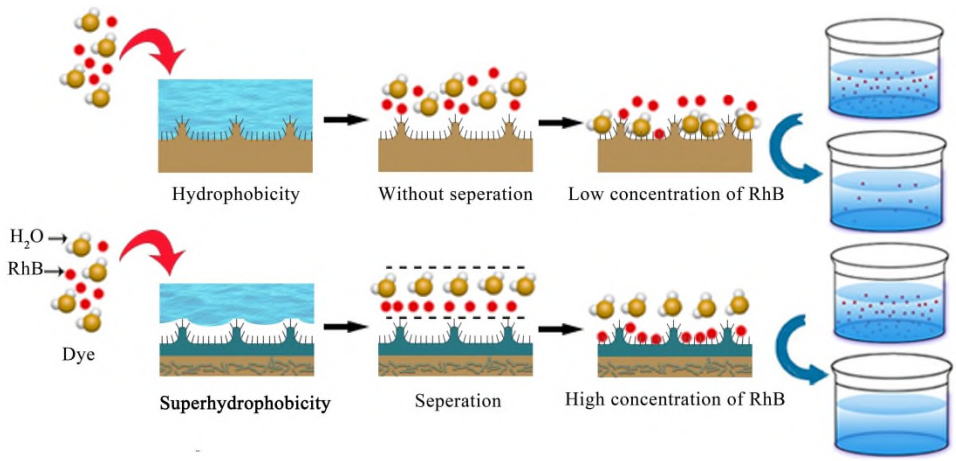

Figure 8 Schematic illustration of the degradation process of RhB with Bi-wood and Bi&F-wood as photocatalysts, respectively.